Chemistry & Biology
Article

Effects of Photochemically Activated Alkylating Agents of the FR900482 Family on Chromatin

Vidya Subramanian,[1] Pascal Ducept,[2] Robert M. Williams,[2,3,*] and Karolin Luger[1,4,*]
[1] Department of Biochemistry and Molecular Biology
[2] Department of Chemistry
Colorado State University, Fort Collins, CO 80523, USA
[3] The University of Colorado Cancer Center, Aurora, CO 80045, USA
[4] Howard Hughes Medical Institute
*Correspondence: rmw@lamar.colostate.edu (R.M.W.), kluger@lamar.colostate.edu (K.L.)
DOI 10.1016/j.chembiol.2007.04.004

SUMMARY

Bioreductive alkylating agents are an important class of clinical antitumor antibiotics that crosslink and monoalkylate DNA. Here, we use a synthetic, photochemically activated derivative of FR400482 to investigate the molecular mechanism of this class of drugs in a biologically relevant context. We find that the organization of DNA into nucleosomes effectively protects it against drug-mediated crosslinking, while permitting monoalkylation. This modification has the potential to lead to the formation of covalent crosslinks between chromatin and nuclear proteins. Using in vitro approaches, we found that interstrand crosslinking of free DNA results in a significant decrease in basal and activated transcription. Finally, crosslinked plasmid DNA is inefficiently assembled into chromatin. Our studies suggest pathways for the clinical effectiveness of this class of reagents.

INTRODUCTION

Many anticancer agents act by impeding rapid proliferation, which is characteristic of cancer cells. While some impact cytoskeletal dynamics and cell-signaling pathways, others affect basic cellular processes such as replication and transcription. Compounds that fall into the latter class include interstrand DNA-crosslinking/DNA-alkylating agents. DNA crosslinking affects DNA-related processes specifically via the formation of covalent bonds between both DNA strands. This is a potent drug-mediated modification associated with severe cytotoxicity [1]. The detailed effects of drug-mediated DNA alkylation on cell proliferation are yet to be determined, since such lesions are likely to be removed and repaired via DNA base-excision repair mechanisms [2, 3].

Bioreductive alkylating agents include families of bifunctional compounds that are capable of forming monoalkylated DNA and interstrand DNA crosslinks under highly reducing conditions. The specific targeting of these drugs to cancer cells has been rationalized by their ability to be activated under the hypoxic conditions that prevail in cancer cells as a result of their high replication rate [4]. A representative clinically significant drug is Mitomycin C (MMC, **1**, Figure 1) [5]. MMC is the most thoroughly studied member of this class of compounds and has been in clinical use for over 30 years as an antitumor agent [6–8]. FR900482 (**2**, Figure 1), a natural metabolite obtained along with FR66979 (**3**, Figure 1A) from *Streptomyces sandaensis* No. 6897, is structurally and functionally related to MMC [9, 10], but it was dropped from clinical development in Phase I studies due to the development of vascular-leak syndrome in patients. More recently, a semisynthetic derivative, FK317, has exhibited promising antitumor activity [10–15] and has advanced from Phase I to Phase II human clinical trials. FK317 (**4**, Figure 1A) shares structural similarities and properties with FR900482 (**2**, Figure 1A), but its use led to fewer side effects, particularly with respect to vascular-leak syndrome, when compared to FR900482 [11, 16].

MMC can be activated via a one-electron or two-electron reduction pathway to form a highly reactive bis-electrophilic mitosene species that is capable of both monoalkylating and crosslinking DNA. In contrast, FR900482 and FK317 are activated specifically by a two-electron reduction pathway to form a structurally and functionally related bis-electrophilic mitosene species (**8**, Figure 1) that is likewise capable of monoalkylating (**10**) and crosslinking DNA (**11**). In all three instances, it has been demonstrated that mitosenes preferentially crosslink B form DNA at 5′CpG3′ steps in the minor groove [17–19]. Mitosene formation appears to be the rate-limiting step in the formation of the final drug-mediated lesion [19]. The solution structure of monoalkylated DNA indicates that the monoadduct represents an intermediate species in a reaction that results in the formation of an interstrand-crosslinked product [20–22]. Recently, we reported a new, to our knowledge, generation of synthetic mitosene progenitors based on FR900482 that can be activated with alternative chemical signals not requiring reductive activation [23]. These agents can potentially obviate the slow generation of the mitosene, and they also allow for controlled release of these highly reactive species. In particular, the totally synthetic NVOC derivative related to FR900482 (**5**, Figure 1) is

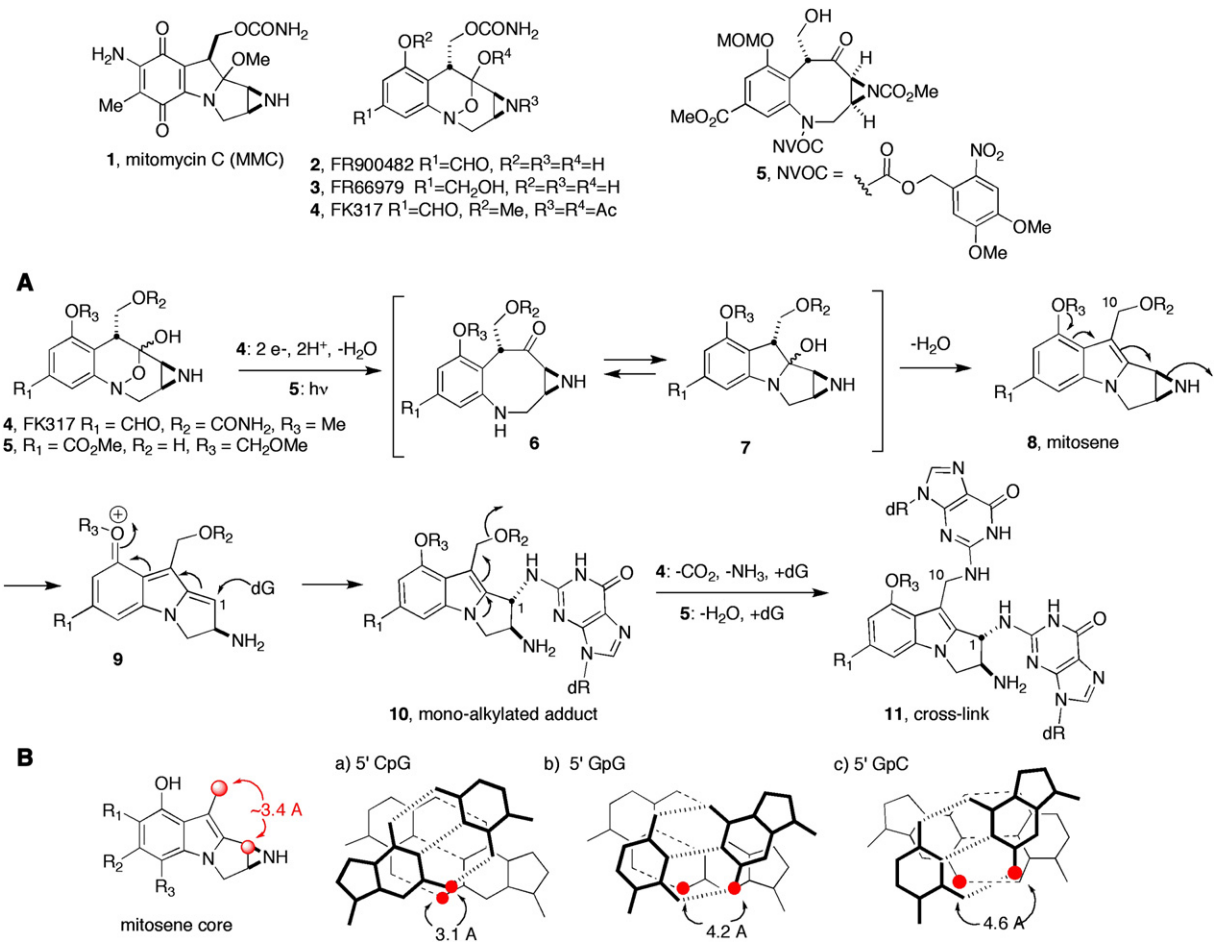

Figure 1. Structure of the Various Mitosene-Based Anticancerous Agents and the Basis for Their Sequence Specificity

(A) Structures of Mitomycin C, FR900482, and congeners. Compound **5** is a photoactivated mitosene progenitor.

(B) Geometrical basis for mitosene-based crosslinking specificity.

activated photochemically and exhibits biochemical reactivity similar to FK317 [23], including the characteristic 5′CpG3′ sequence specificity for interstrand crosslinking.

The striking preference of all mitosene-based drugs for crosslinking 5′CpG3′ steps is thought to be due to the geometrical arrangement of the two electrophilic sites on the mitosene, which closely aligns with the distance between the opposing dG residues at a 5′CpG3′ step in B form DNA (Figure 1B). This requirement has been shown to be less stringent for monoalkylation [20, 24]. While the sequence specificity for both monoalkylation and interstrand crosslinking was originally determined on free B form DNA [25], the interactions of this class of drugs with DNA in the context of nucleosomes have not been studied in detail. This is a significant concern since ~80% of all eukaryotic DNA is organized into nucleosomes. Nucleosomal DNA conformation deviates significantly from that of unassembled B form DNA, and, as such, the identification of the covalent interactions of these drugs in an environment more closely resembling that of chromosomal DNA as packaged in the nucleus of living cells is particularly relevant. A previous study revealed a decrease in the levels of MMC-mediated interstrand crosslinking on nucleosomal DNA when compared to free DNA [26]; however, MMC-mediated monoalkylation on linear versus nucleosomal DNA could not be demonstrated conclusively. Furthermore, the effects of DNA crosslinking on transcription and chromatin assembly have not been investigated in detail.

Here, we describe the effect of a photochemically activated NVOC derivative (**5**, Figure 1) on two distinct free and nucleosomal DNA templates that are both 146 bp in length. Apart from base composition, the templates differ in the number and location of 5′CpG3′ steps (Figure 2). We investigated the ability of **5** to crosslink or alkylate free and nucleosomal DNA. We observed a dramatic decrease in crosslinking of nucleosomal DNA and a commensurate increase in monoalkylation. Compound **5** significantly inhibits in vitro transcription and nucleosome assembly. Our studies conclude that crosslinking of free DNA mediated by **5** may affect cellular proliferation by targeting two vital processes—chromatin assembly and transcription.

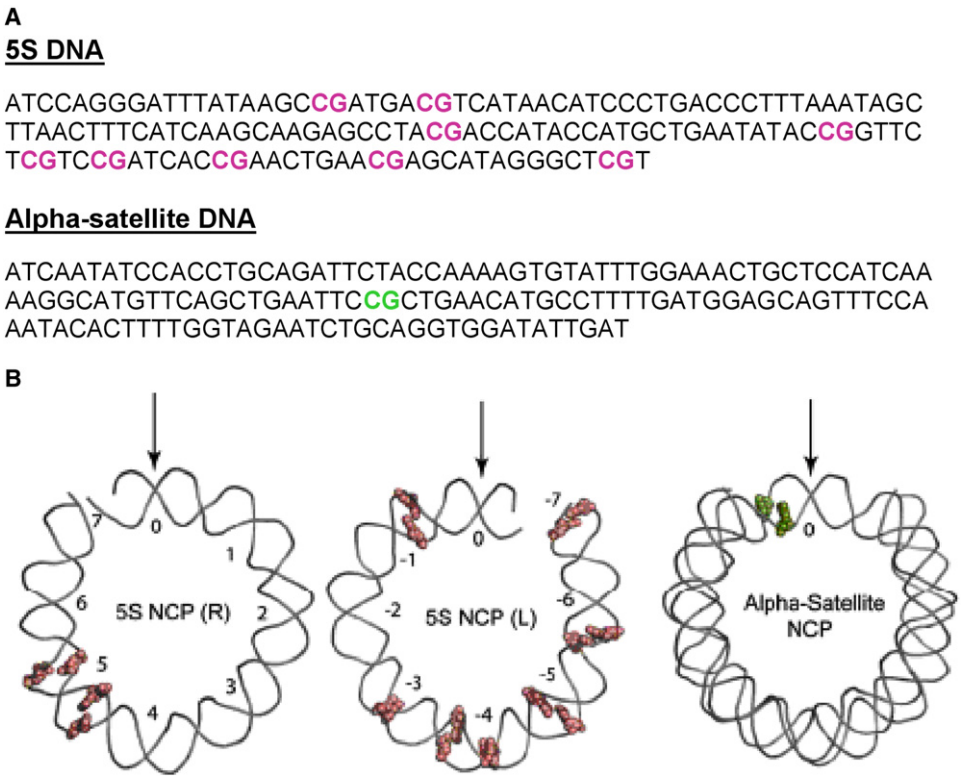

Figure 2. The Two DNA Fragments Differ in the Number and Location of 5′CpG3′ Dinucleotide Steps

(A) Sequence of the two DNA fragments under investigation. The asymmetric 5S DNA template contains nine 5′CpG3′steps (pink); the palindromic α-satellite DNA contains a single 5′CpG3′step (green).

(B) Representation of a target site in a structural context. The left and middle panels represent the two halves of the 5S DNA (5S NCP [R] and [L], respectively); the dyad is indicated as 0. The numbers ± 1–7 represent the superhelical axis location (SHL) of nucleosomal DNA. Since the structure of the 5S NCP is not known, we show a projection of the target sites onto the structure of the α-satellite NCP as a model. The right-most panel is a graphical representation of the compound **5** target site on α-satellite nucleosomal DNA. The arrows indicate the location of the symmetry dyad.

RESULTS

Nucleosomal DNA Is Crosslinked Inefficiently by Compound 5 Compared to Free DNA

The preference of mitosene-based drugs for 5′CpG3′ dinucleotide steps results from the favorable geometric arrangement of the electrophilic sites of the drug and the target sites on linear B form DNA (Figure 1). Nucleosomal DNA, although still classified as B form, is distorted compared to unassembled DNA due to the high degree of bending upon superhelix formation [25]. To test the effect of this distortion on the efficiency of crosslinking, we compared two different 146 bp DNA sequences in the context of highly positioned nucleosomes—a palindromic DNA fragment derived from human α-satellite DNA and an asymmetric fragment derived from the *Xenopus laevis* 5S rRNA gene. While the former has been used routinely to generate homogeneous nucleosome species mainly for crystallization purposes (reviewed in [27]), the latter has been used extensively for biochemical analyses. The two sequences differ significantly in the number and location of 5′CpG3′ steps (Figure 2).

Free DNA and assembled nucleosomes (5S and α-satellite nucleosome core particle [NCP]) that had been separated from any remaining free DNA by preparative gel electrophoresis were treated with **5** and were analyzed by native PAGE for the presence of free DNA (Figures 3A and 3B). Even at a 60-fold molar excess of **5**, nucleosomes remained intact and exhibited no release of free DNA. DNA was isolated from nucleosomes, and the degree of crosslinking in free and nucleosomal DNA was analyzed by alkaline agarose electrophoresis (Figures 3C–3F). The percentage of crosslinks as a function of molar excess of drug is plotted in Figure 3G. As expected from the differences in the number of 5′CpG3′ sites on α-satellite DNA compared to 5S DNA (1 versus 9 in each 146 bp DNA fragment, Figure 2), free 5S DNA is crosslinked much more efficiently than free α-satellite DNA (Figure 3C versus Figure 3D, respectively). In both cases, the level of crosslinking is reduced significantly in nucleosomes (Figures 3E and 3F for 5S NCP and α-satellite NCP, respectively), indicating that the inherent distortions in nucleosomal DNA and the partial protection by histones inhibit the formation of interstrand crosslinks.

Similar experiments were also performed with the FK317 compound (**4**, Figure 1). The rate of FK317-mediated modification was exceedingly slow, requiring as long as

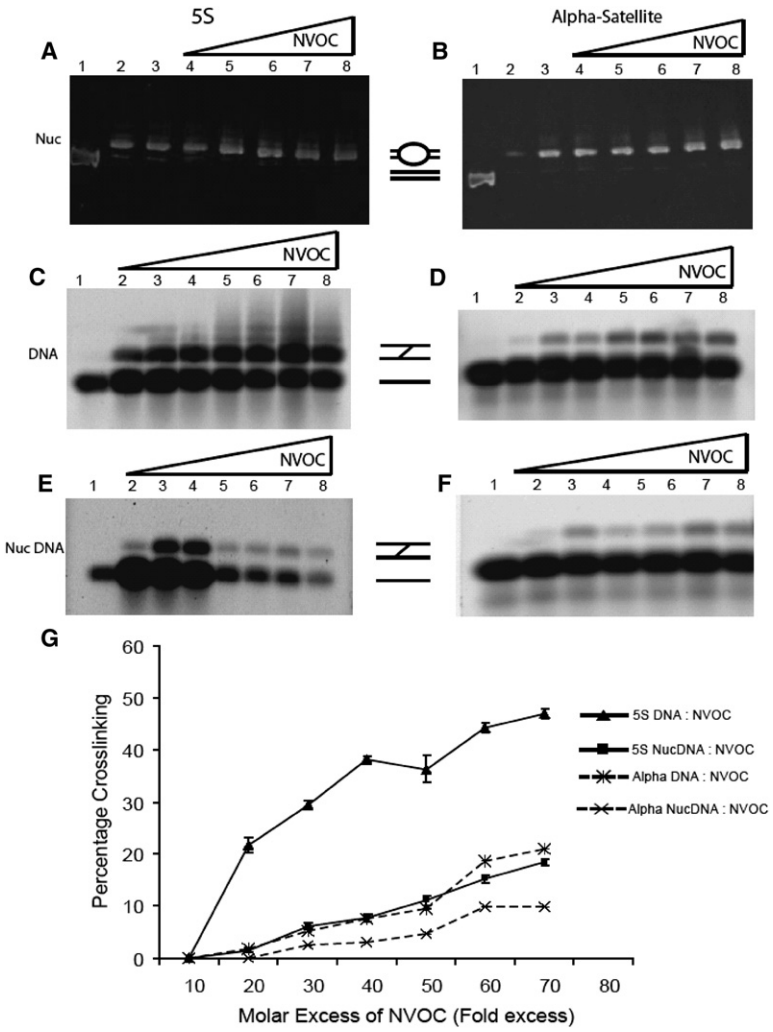

Figure 3. Reduced Crosslinking Mediated by the NVOC Derivative 5 on Nucleosomal DNA

(A and B) NCPs reconstituted with 5S DNA and α-satellite DNA, respectively, treated with increasing molar ratios of NCP:compound **5**. The samples were analyzed on a 5% native PAGE gel stained with ethidium bromide to determine any appearance of free DNA due to compound **5**-induced NCP dissociation. Lane 1 in (A) and (B) indicates free DNA, while lane 2 in both panels shows NCP controls without the drug. Lane 3 shows NCP treated with UV radiation without the drug, while lanes 4–8 show 1:1, 1:10, 1:20, 1:40, and 1:60 ratios, respectively, of NCP:compound **5** in both panels. (C–F) (C) and (D) show denaturing alkaline agarose gels of 5S and α-satellite DNA treated with increasing ratios of NCP:compound **5**. Lane 1 in both panels shows untreated DNA, while the DNA in lanes 2–8 was treated with 1:1, 1:5, 1:10, 1:20, 1:40, 1:60, and 1:80 molar ratios, respectively, of NCP:compound **5**. (E) and (F) show denaturing alkaline agarose gels of 5S and α-satellite nucleosomal DNA treated with increasing ratios of NCP:compound **5**. Lane 1 in both panels represents untreated DNA, while lanes 2–8 represent 1:1, 1:5, 1:10, 1:20, 1:40, 1:60, and 1:80 ratios, respectively, of NCP:compound **5**. The alkaline agarose gels were stained and visualized with Sybr Gold, and the intensity of the crosslinked and uncrosslinked bands was determined by using the Image Quant Analysis (version 5.1) software. (G) Graphical representation of the efficiency of compound **5**-mediated crosslinking on DNA/nucleosomal α-satellite and 5S DNA. The efficiency of crosslinking was determined from the ratio of the intensity of the crosslinked band to the sum of the intensities of the crosslinked and uncrosslinked bands, and values thus obtained were plotted as compound **5**-mediated percentage crosslinking as a function of the fold excess of compound **5** (over DNA/nucleosomal DNA).

3 months after activation of the drug to obtain detectable levels of crosslinking on free 5S DNA. No detectable levels of crosslinks were observed on either 5S NCP or unassembled and assembled α-satellite DNA (data not shown). Since the integrity of nucleosome samples for such extended periods of time was uncertain, further studies with this compound were deemed impractical.

Alkaline agarose gel electrophoresis allows us to distinguish between crosslinked and uncrosslinked species, but it does not possess the resolution to visualize monoalkylation. In contrast, denaturing PAGE allows for good resolution of the unmodified, single-stranded DNA; monoalkylated, single-stranded DNA; and crosslinked DNA strands. Figure 4A shows the analysis for free and nucleosomal α-satellite DNA. A crosslinked DNA control, purified from a denaturing gel, was loaded as a control (Figure 4A, lane 2). The gel was scanned, and the percentage of crosslinked DNA obtained by this method was compared to the numbers plotted in Figure 3G. The numbers obtained for a 40-fold molar excess of compound **5** (1.2% and 14% for nucleosomal and free α-satellite DNA, respectively) compared well to numbers plotted in Figure 3G (4.5% and 11%, respectively).

Even though the α-satellite DNA template has only one 5′CpG3′ site (Figure 2), two bands are visible in Figure 4A upon incubation with compound **5**. Although we cannot exclude the possibility that these represent adducts formed at other sites, we surmised that these may represent positional crosslinked isomers. These isomers may be formed due to the difference in orientation of the reactive mitosene residue in the 5′CpG3′ step, which is largely dependent on which of the reactive centers on the mitosene moiety reacts with the exocyclic N2 amine on guanosine [18]. The nucleosomal template has a much higher abundance of the monoadduct than free DNA, demonstrating that nucleosomal DNA is preferentially monoalkylated. Since only a single monoalkylated species is apparent, we suggest that the sequence preference for 5′CpG3′

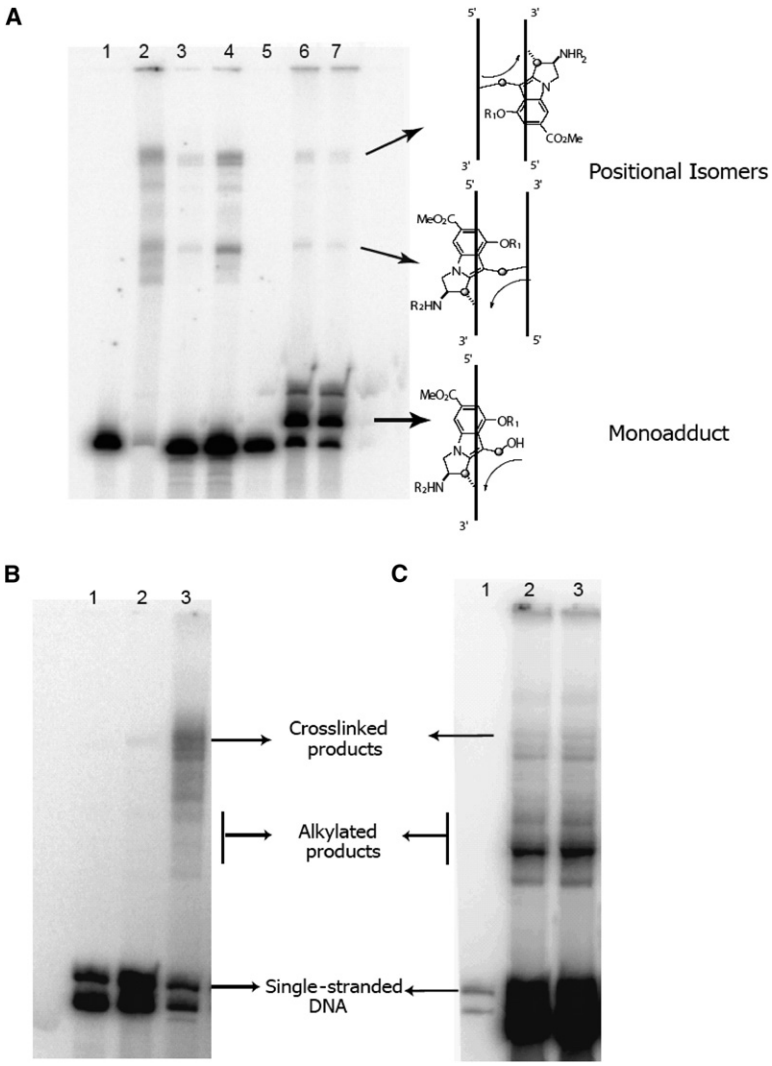

Figure 4. Preferential Compound 5-Mediated Monoalkylation of Nucleosomal DNA Compared to Linear DNA

(A–C) Urea-8% polyacrylamide gel (8% DPAGE) analysis was conducted on [γ-^{32}P]ATP nucleosomal and free DNA. (A) DPAGE analysis on compound **5**-treated α-satellite DNA/nucleosomal DNA. Lane 1, α-satellite DNA; lane 2, crosslinked α-satellite DNA control. The two different orientation isomers are illustrated at the side of the gel. Lanes 3 and 4, α-satellite DNA treated with a 20 and 40 molar excess, respectively, of compound **5** to DNA. Lane 5, nucleosomal α-satellite DNA treated with Proteinase K; lanes 6 and 7, nucleosomal DNA treated with 20 and 40 molar excess, respectively, of compound **5**. (B) DPAGE analysis of free 5S DNA. Lane 1, 5S DNA. The two bands correspond to the difference in charge, and hence migration, of the two complimentary strands of 5S DNA. Lanes 2 and 3, 5S DNA treated with 20 and 40 molar excess, respectively, of compound **5**. (C) DPAGE analysis of 5S nucleosomal DNA. Lane 1, nucleosomal 5S DNA treated with Proteinase K; lanes 2 and 3, nucleosomal 5S DNA treated with 20 and 40 molar excess, respectively, of compound **5**. The concentration of DNA used in these reactions was 6.25 μM, and that of the nucleosomes was 12.5 μM.

may be maintained in the context of the nucleosome even for monoalkylation by **5**.

The same experiment was repeated with 5S DNA, which contains nine (as opposed to one) 5′CpG3′ sites. No significant monoalkylated species were observed on free 5S DNA at a 40-fold molar excess of drug (Figure 4B, lane 3). Instead, we observed a family of multialkylated products whose migration rates are slower than the monoadduct species, but faster than the more prominent crosslinked species. Nucleosomal 5S DNA treated with similar amounts of **5** is predominantly multialkylated, whereas crosslinks are barely visible (Figure 4C, lanes 2 and 3). We conclude that the NVOC derivative **5** is bifunctional and can cause both interstrand DNA crosslinking as well as alkylation. The outcome apparently depends entirely on the conformational state of the DNA.

The presence of monoalkylated DNA raises the intriguing possibility that histones may become crosslinked to DNA upon treatment with **5**. However, preliminary assays in which dissociation of nucleosomes in response to salt was measured showed no difference between untreated and **5**-treated nucleosomes, indicating that no protein-DNA crosslinks were formed. This was not entirely unexpected since the distances between lysines and DNA bases in the nucleosome structure are too large for effective crosslinks. However, more careful analysis is required to exclude the possibility of drug-mediated histone-DNA-induced crosslinks.

Compound 5-Mediated Crosslinking of Unassembled DNA Represses In Vitro Transcription

Histones are transiently removed from DNA during transcription, often with the help of ATP-dependent chromatin-remodeling factors and perhaps also histone chaperones [28, 29]. This generates a window of opportunity for efficient crosslinking of nucleosome-free DNA by mitosene-based drugs. To investigate the effect of crosslinking on basal and activated transcription, we employed a previously established in vitro system [30, 31] that utilizes a well-characterized plasmid template (p4TxRE/G-less). The plasmid contains 178 5′CpG3′ dinucleotide steps that are distributed quite uniformly along its entire length,

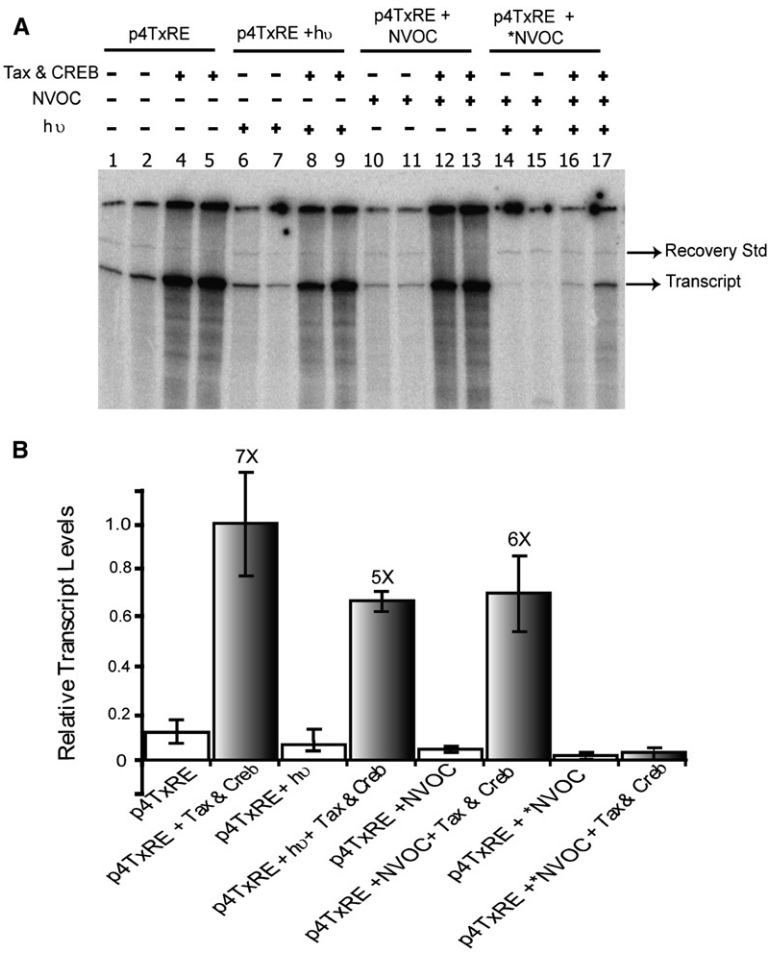

Figure 5. Decreased Levels of In Vitro Transcription from Crosslinked DNA Templates

(A) In vitro transcription assay indicating a decrease in transcript levels only in the presence of compound **5**-mediated crosslinked product. The asterisk indicates activated compound **5**. Each transcription reaction contains 150 ng p4TxRE template and 60 μg nuclear extract-CEM from HTLV-negative human T cells. A total of 100 ng purified recombinant Tax and 100 ng purified recombinant CREB were added to the reaction where indicated.

(B) Quantitation of the transcript levels was performed by using Image Quant Analysis (version 5.1) software, and the relative transcript levels were normalized to the highest Tax and CREB activation. The shaded bars represent those reactions activated by Tax and CREB. The fold increase in transcription levels due to this activation (compared to the corresponding basal transcription levels, empty bars) is indicated above each of these bars. The error bars represent the deviation from the average transcript levels obtained from three independent experiments.

with the exception of the 380 bp G-less cassette. We made use of an in vitro assembly system consisting of purified assembly factors that recapitulates many aspects of in vivo chromatin assembly [30].

Transcript levels were monitored under basal and activated conditions in the absence and presence of the coactivators Tax and CREB [32]. To account for variations in the recovery of transcripts, each reaction was normalized against a recovery standard (see Experimental Procedures). Under both conditions, the crosslinked template showed a significant reduction in transcription levels when compared to a control that had not been activated by light. Figure 5B is a quantitative representation of the data shown in Figure 5A. Basal transcript levels from crosslinked DNA template decreased 5-fold compared to untreated template. Activated transcript levels dropped 25-fold when compared to the transcript levels of the inactive-compound **5** reaction.

Compound 5-Mediated Crosslinking of Plasmid DNA Reduces the Efficiency of Chromatin Assembly

Mitosene-based drugs are particularly effective in rapidly dividing cancer cells, where DNA synthesis and concomitant chromatin assembly are frequent events. We therefore wanted to quantify the effect of DNA crosslinking and alkylation on the efficiency of in vitro chromatin assembly. The same p4TxRE/G-less templates (untreated and treated with compound **5**) that were used for the in vitro transcription assay described above were employed for this assay.

The plasmid was treated with a 40-fold molar excess of compound **5** prior to assembly to ensure complete saturation of all available sites. Crosslinking was verified by linearizing the plasmid, followed by analysis by alkaline gel electrophoresis (data not shown). Crosslinked plasmid was purified from unreacted DNA and free **5** by gel elution under native conditions, exploiting the fact that crosslinked plasmid exhibits a slower electrophoretic mobility than untreated plasmid (data not shown). Untreated and **5**-treated supercoiled plasmids were assembled into chromatin by using the purified chromatin-remodeling factor ACF1 and the histone chaperone dNAP-1 [33]. The assemblies were assayed by micrococcal nuclease (MNase) digestion and Quantitative Agarose Gel Electrophoresis (QAGE)-Multigel Analysis.

MNase digestion confirmed that the nucleosomes reconstituted onto untreated DNA template are spaced, on average, 165–170 bp apart (Figure 6A, lanes 2–5). Interestingly, chromatin assembled on **5**-treated plasmid DNA was resistant toward digestion with MNase, whereas no

effect was found if the plasmid was treated with light in the absence of **5**. A DNA band corresponding to mononucleosomes was visible only at the highest MNase concentrations (Figure 6A, lane 15). This could be due to the fact that crosslinked DNA is a poor substrate for most nucleases [33]. This was addressed in a control experiment in which the effect of **5** treatment on the sensitivity of unassembled plasmid DNA to digestion with MNase was assayed (Figure 6A, right panel). Whereas untreated DNA is digested rapidly and without a trace, crosslinked plasmid DNA exhibited increased resistance toward digestion.

The results shown in Figure 6A raise the possibility that chromatin assembly is inefficient on a crosslinked DNA template. To further investigate this, we used QAGE-Multigel Analysis, a method that has been used successfully in the past for the analysis of chromatin to determine parameters such as average surface charge density and particle deformability [34, 35]. More precisely, this method allows us to quantitate the average surface charge density of unassembled DNA and assembled DNA, thus effectively "counting" the number of nucleosomes on any given DNA fragment. The same analysis was also performed with the free DNA sample. A typical example is shown in Figure 6B. Ferguson plots (semilogarithmic plots of migration distance, μ, versus agarose percentage; Figure 6C) allow for the determination of μ_o and μ_o'. The μ_o' values for all of the species in Figure 6 are listed in Table 1. Crosslinked DNA species and the untreated DNA species do not vary significantly in their μ_o' values. This demonstrates that there are no differences in surface charge densities in the free DNA upon treatment with compound **5**. This not only validates the technique, but also establishes the fact that any change in nucleosome assembly on the **5**-treated and untreated plasmid is not associated with charge.

The μ_o' values listed in Table 1 were used to calculate the number of nucleosomes assembled on the two templates [34, 35]. This analysis shows that an average of 18.5 nucleosomes are assembled on the untreated p4TxRE/G-less plasmid. On 3245 bp, this converts to a repeat length of 175 bp, a number that corresponds well to the repeat length established by MNase (Figure 6A, left panel). On crosslinked DNA, an average of 14.5 nucleosomes was assembled. This 22% reduction in the number of nucleosomes assembled on the **5**-treated DNA template when compared to an untreated DNA template is reproducible and indicates that crosslinking indeed has an inhibitory effect on chromatin assembly under physiological conditions.

DISCUSSION

Bioreductive alkylating agents are an important class of anticancer drugs that act through their ability to covalently crosslink two strands of DNA, thus impeding DNA replication of rapidly dividing cancer cells. The synthetic NVOC derivative (**5**) is a photoactivated compound that generates in high chemical yield a doubly electrophilic mitosene species that is structurally and mechanistically homologous to the mitosenes generated by bioreductive activation of FK317, MMC, and congeners. Here, we showed that interstrand crosslinking of nucleosomal DNA by compound **5** is suppressed, while, at the same time, the extent of monoalkylation markedly increases. Our finding that crosslinked DNA is inefficiently transcribed and assembled into chromatin suggests additional mechanisms by which mitosene-based drugs display their cytotoxic effect.

It has been shown previously that the efficiency of MMC-induced crosslinking on nucleosomes, compared to free DNA, was reduced [26]. In the present study, we have significantly extended this finding by demonstrating the preferential formation of monoalkylated over crosslinked products at the nucleosomal dyad. Nucleosomal DNA is distinct from unassembled DNA in its helical parameters [25]. The exact geometry of each given CpG step depends on its rotational and translational position with respect to the histone octamer. By using nucleosomes assembled on α-satellite DNA, we have the opportunity to directly measure the distance between the reactive centers of the only CpG step that is located near the nucleosomal dyad [36]. The distance measured between the two opposing exocyclic amine residues in the minor groove at this particular location in the nucleosome is 3.95 Å, whereas the distance between the same reactive centers on unassembled B form DNA is 3.4 Å. This 0.5 Å difference is significant in light of the estimated distances between reactive centers in other dinucleotides that are not crosslinked on B form DNA. For example, the distance between the targets sites in a GpG step is ~4.2 Å, and in a GpC step it is ~4.6 Å.

Apparently, nucleosomal DNA is too structurally constrained to allow for mitosene-mediated interstrand crosslinking. Instead, monoalkyation at presumably the same site is observed. What then is the biological significance of mitosene-mediated alkylation of nucleosomal DNA? Alkylation has been considered a less cytotoxic modification compared to interstrand DNA crosslinking, as it is easily corrected by the nucleotide base-excision repair machinery [2, 3]. However, it remains to be investigated how efficiently this type of damage is repaired in the context of chromatin. Monoalkylation has also been proposed as a suitable intermediate for the formation of crosslinks. Earlier studies have shown that congener FR66979 can cause protein-DNA crosslinks via drug-mediated monoalkylation of DNA and the oncoprotein HMG A1 in vitro [37]. Similar crosslinks were observed in vivo upon treatment with FR900482 and FK317 [38]. This leads to the interesting hypothesis that monoalkylation of nucleosomal DNA, especially at the nucleosomal dyad, could result in the crosslinking of chromatin-associated protein to nucleosomal DNA, which could have far-reaching implications on chromatin dynamics and DNA accessibility.

About 80% of all eukaryotic DNA is organized in nucleosomes, leaving only parts of the linker DNA and the occasional highly active promoter histone free. The processes of replication, transcription, and DNA repair require transient exposure of DNA [39, 40]. This may represent

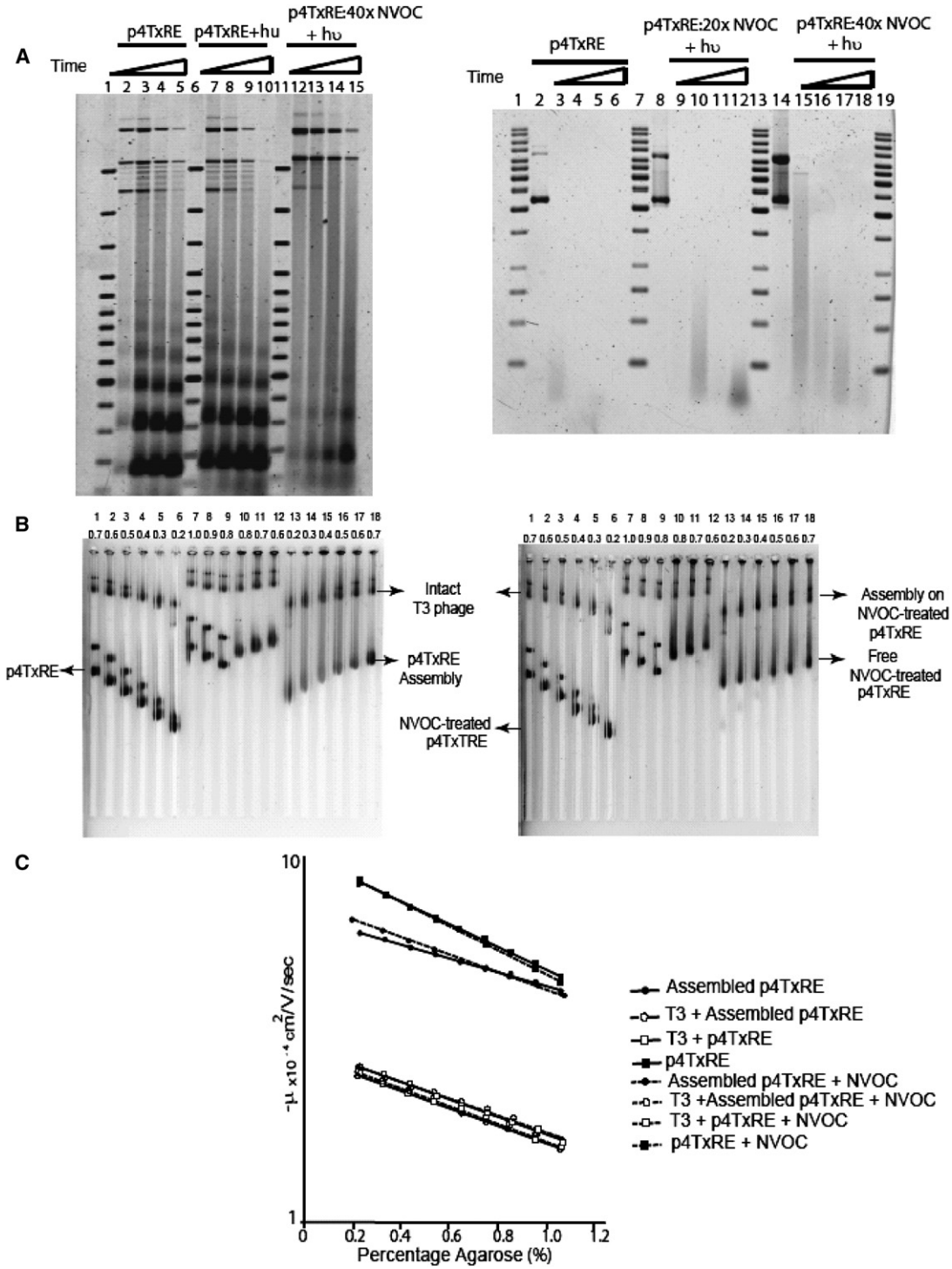

Figure 6. Crosslinking of DNA Affects the Efficiency of Chromatin Assembly

(A) Qualitative analysis of the assembled template by micrococcal nuclease digestion. The various templates used in these analyses are indicated above the lanes. The left panel represents the micrococcocal nuclease digestion on chromatin templates at different time points (1, 2, 4, and 8 min, respectively). The right panel represents the micrococcal nuclease digestion analyses on untreated and compound **5**-treated p4TxRE. Lanes 2, 8, and 14 represent untreated p4TxRE, p4TxRE treated with 20 molar excess compound **5**, and p4TxRE treated with 40 molar excess compound **5**, respectively. Lanes 3–6, 9–12, and 15–18 represent the digestion times of 0.5, 1, 2, and 4 min, respectively.

(B) The right and left panels represent the QAGE analyses performed on untreated p4TxRE/assembled p4TxRE and compound **5**-treated p4TxRE/assembly with crosslinked p4TxRE, respectively. The numbers over each lane indicate the agarose concentrations.

A qualitative representation of these data is shown in Table 1.

Table 1. Quantitative Analysis of Chromatin Assembly via Multigel Analysis

Samples	μ_o cm^2/V/s ($\times 10^{-4}$)	Number of Nucleosomes
p4TxRE/G-less	−2.27635	
Assembled p4TxRE/G-less	−1.6764	18.5 ± 2
Compound **5**-treated p4TxRE/G-less	−2.47647	
Assembled, compound **5**-treated p4TxRE/G-less	−1.9661	14.5 ± 1

The number of nucleosomes was calculated as described in Experimental Procedures. Experiments were repeated three times.

a window of opportunity for mitosene-derived drugs to crosslink the two strands of DNA. This modification is likely to be refractory to all processes that require melting of the DNA double helix. Our studies show that basal as well as activated transcription from crosslinked DNA templates is severely impaired. This defect stems from the inability of the polymerase to initiate transcription, since the G-less cassette is free of crosslinks.

The potential effect of DNA crosslinking on chromatin assembly has largely been ignored in investigations of the mechanisms of mitosene-based cytotoxicity. Using a defined in vitro assembly system, we found a 22% decrease in nucleosome occupancy on a crosslinked template. The majority of chromatin is assembled during S phase, during which the histones are deposited on the newly replicated DNA by Chromatin Assembly Factor-1 (CAF-1) [41]. Suppression of the p60 subunit of CAF-1 by RNAi results in a slightly reduced efficiency of chromatin assembly [42]. These cells exhibited cell-cycle arrest and programmed cell death. Thus, it appears that a relatively small decrease in assembly could be a sufficient signal to induce cell-cycle arrest in S phase, especially in rapidly dividing cells. Since posttranscriptional chromatin assembly is also a key process for quiescent cells, it is possible that mitosenes may be toxic for nondividing cells through these mechanisms.

To our knowledge, these studies reveal new and hitherto unresolved possible mechanisms to explain how mitosene-based antitumor agents may exert their cytotoxic effect in rapidly proliferating cells. We are continuing to study the molecular interactions of such agents in the context of dynamic processes of chromatin assembly, and there remains the possibility for the formation of additional covalencies between the DNA-bound drug and histones as well as other proteins closely associated with the complex processes of replication and transcription.

SIGNIFICANCE

This study has been able to emphasize the differential activity of the phototriggered NVOC derivative on conformationally distinct unassembled and assembled DNA. The bifunctional activity of compound 5 seems to be dependent on the conformation of the DNA template. We believe that this finding will help provide insight into the design of a specific alkylating agent based on the contours of nucleosomal DNA and hence into its effective use as an anticancerous agent.

This study has also shown conclusively the effect of compound 5-mediated interstrand crosslinking on transcription and chromatin assembly. We believe that this is the first time the quantitative effect of crosslinking on both of these functional processes has been demonstrated. This could be a major step in understanding one of the many levels at which these DNA crosslinking agents act to decrease and disrupt cellular replication, and hence behave as effective anticancerous drugs.

EXPERIMENTAL PROCEDURES

Drug Stock Solution

Compound **5** was prepared according to published procedures [23]. A stock solution of 10 mg/ml (15.8 mM) **5** was prepared in 100% DMSO and placed in a light-safe tube to prevent photodecay. Appropriate dilutions were made in 100% DMSO.

Nucleosome Preparation

The 146 bp 5S and α-satellite DNA templates were prepared as published [43], and the corresponding nucleosomes were reconstituted by using recombinant full-length *Xenopus* histone octamer via salt dialysis as described earlier [27].

DNA Crosslinking and Alkaline Agarose Electrophoresis

The final volume of the crosslinking reaction was 20 μl. The final concentration of free DNA (both 5S and α-satellite) in these reactions was 6.25 μM, and it was 12.5 μM for nucleosomal DNA. The samples were irradiated in clear Eppendorf tubes at 25°C for 1 hr with an ultraviolet lamp (Rayonet) containing 350 nm bulbs [23, 44] and incubated in the dark at 4°C. Excess drug was removed from free DNA samples by ethanol precipitation. In order to remove excess drug and histones from compound **5**-treated nucleosomal samples, the 20 μl reaction mixture was treated with 5.2 μl 4M NaCl, 4 μl 20 mg/ml glycogen, and 60 μl 100% ethanol. The nucleosomes were then pelleted by spinning the samples at 13.2 K rpm for 30 min. Histones were removed by Proteinase K treatment in a volume of 100 μl containing a final concentration of 0.1 mg/ml Proteinase K (Sigma-Aldrich). The samples were incubated at 37°C for at least 1 hr, followed by phenol chloroform extraction and ethanol precipitation. All samples (both nucleosomal and free DNA) were analyzed by 1.4% alkaline agarose electrophoresis [45]. The gels were run at 75 V for 50–55 min and stained with SyBr Gold (Invitrogen, Molecular Probes). The appropriate bands were quantified by using Image Quant Analysis (version 5.1) software.

(C) The QAGE results are represented quantitatively in a Ferguson Plot. The y axis has been set to logarithmic scale. Intact T3 phage was used as a migration control as well as in determination of the unknown μo value for unassembled and assembled DNA. The plot is first used to determine the gel-free mobility (μo′) [35]. The values obtained in these plots are listed in Table 1.

Analysis of Monoalkylation

Free and nucleosomal DNA samples were subjected to treatment with compound **5**, and DNA was isolated from nucleosomes as described above. A total of 10 μg extracted DNA was radiolabeled at the 5′ end with [γ-^{32}P]ATP by following standard protocols in a final volume of 50 μl and in the presence of T4 polynucleotide kinase (NEB). The radiolabeled DNA was then subjected to phenol-chloroform extraction and ethanol precipitation to remove enzyme and excess radiolabel in the reaction mix. The resulting samples were analyzed by 8% PAGE in the presence of urea [44]. The gel was first prerun at 30 W for about 30 min (until the temperature of the gel was ~50°C), and then run at 30 W for 40 min in 1× TBE buffer. The gel was dried and exposed to a Phosphorimager screen for 10–15 hr. The screen was then scanned and visualized with Image Quant Analysis (version 5.1) software.

In Vitro Chromatin Assembly

The p4TxRE/G-less plasmid template, native *Drosophila* core histones, recombinant ACF, and dNAP1 were purified as described [30]. The in vitro assemblies were performed as described in [30]. The standard chromatin assembly reaction was 98 μl and contained 2.1 μg plasmid DNA (0.994 pmoles 3.2 kp plasmid DNA), 1.505 μg purified native *Drosophila* core histones (0.11 nmoles of each histone), 12.012 μg purified recombinant dNAP1 (0.2145 nmoles dNAP1 monomer), and 0.36 μg purified recombinant *Drosophila* ACF (1.285 pmoles ACF peptide), in 10 mM HEPES (pH 7.6), 50 mM KCl, 5 mM $MgCl_2$, 5% glycerol, 1% PEG, 3 mM ATP, 0.01% NP40, an ATP-regenerating system (30 mM phosphocreatinine and 1 μg/ml creatinine phosphokinase), and 140 ng BSA. The reaction was performed at 27°C for 4–12 hr. Micrococcal nuclease digestion was performed as described [46].

Quantitative Agarose Gel Electrophoresis-Multigel Analysis

To determine the number of assembled nucleosomes, the average surface charge density of unassembled and assembled DNA template had to be quantitated [34]. The mobility of the species (μ) was calculated as a function of the agarose concentration in electrophoresis performed on nine gels, each of different concentrations, between 0.2% and 1.0%, of agarose, embedded in a 1.5% agarose frame and run at 1 V/cm. The values of μ_o' (gel free mobility) and μ_o (μ_o' corrected for the electro-osmotic effects of the buffer) were estimated as described [35]. In this study, the 18-lane template was used to run unassembled DNA with its corresponding assembled species in the same gel frame. Both the frame and running gel were cast in TAE buffer (40 mM Tris acetate, 1 mM EDTA [pH 7.8]) or E Buffer (40 mM Tris-HCl, 0.25 mM EDTA [pH 7.8]) as indicated, and the corresponding EEO (electroendoosmosis) values were used to calculate μ_o. The assembly reaction containing 2.1 μg assembled DNA along with 1 μg intact T3 phage (migration standard) was loaded such that 0.23 μg assembled DNA was present in each well. The same amount of supercoiled unassembled DNA was loaded along with the T3 control. The gels were run at room temperature (48 V for 6 hr), with running buffer circulating for the duration of the experiment. With the μ_o values thus obtained for unassembled and assembled DNA templates, the number of assembled nucleosomes was calculated as reported [34, 35].

The p4TxRE/G-less plasmid was treated with compound **5** in a manner similar to that of unassembled DNA, as mentioned previously in the same section.

In Vitro Transcription Assay

The in vitro transcription assay was carried out in a final reaction volume of 30 μl containing 1 mM acetyl CoA, 150 ng DNA (treated or untreated as mentioned), and 70 μg CEM (HTLV-negative human T cells). For activated transcription reactions, the same conditions were used along with 100 ng Tax and 100 ng CREB. The reactions were incubated at 30°C for 1 hr. The samples were then incubated with 250 μM ATP, 250 μM CTP, 12 μM UTP, and 0.8 μM [α-^{32}P]UTP (3,000 Ci/mmol) for 30 min at 30°C. This allows for transcription through the 380 nt G-less cassette in the p4TxRE/G-less plasmid [31]. The readthrough transcripts were cleaved after treating these reactions with RNase T1 (100 U/reaction) at 37°C for 30 min. RNase T1 is an endoribonuclease that specifically degrades single-stranded RNA at the G residues. This enzyme is therefore extremely useful for detection of RNA transcript levels from DNA templates containing the G-less cassette. The reaction was terminated by addition of 123 mM NaCl, 0.5% SDS, and 2.5 mM EDTA, and the samples were subjected to Proteinase K treatment at 50°C for 30 min. The transcripts were then extracted via precipitation with a final concentration of 0.48 M ammonium acetate and 0.3 mg/ml carrier tRNA. In this step, an appropriate amount of radiolabeled DNA fragment was added as a recovery standard. The precipitated samples were analyzed on a urea-6.5% polyacrylamide gel. The gel was subsequently dried and visualized by Image Quant Analysis (version 5.1) software. The software was used to quantitate the transcript yields under the various conditions indicated. The transcript levels in each lane were normalized against the recovery standard (internal control). The highest signal (due to activation with Tax and CREB) was assigned the number 1, and all the other normalized transcript levels were then represented as fractions of the highest value.

ACKNOWLEDGMENTS

We thank Drs. Konesky, Lu, Nyborg, and Stargell for guidance and reagents, and P.N. Dyer for help with histone and DNA preparation. We thank Fujisawa Pharmaceutical Co. (now Astellas) for the generous gift of FK317. This work was financially supported by National Institutes of Health RO1 GM061909 to K.L., and by RO1 CA51875 to R.M.W. K.L. is an Investigator with the Howard Hughes Medical Institute.

Received: January 30, 2007
Revised: March 16, 2007
Accepted: April 4, 2007
Published: May 29, 2007

REFERENCES

1. Zwelling, L.A., Anderson, T., and Kohn, K.W. (1979). DNA-protein and DNA interstrand cross-linking by cis- and trans-platinum(II) diamminedichloride in L1210 mouse leukemia cells and relation to cytotoxicity. Cancer Res. *39*, 365–369.
2. Lawley, P.D., Lethbridge, J.H., Edwards, P.A., and Shooter, K.V. (1969). Inactivation of bacteriophage T7 by mono- and difunctional sulphur mustards in relation to cross-linking and depurination of bacteriophage DNA. J. Mol. Biol. *39*, 181–198.
3. Sancar, A. (1996). DNA excision repair. Annu. Rev. Biochem. *65*, 43–81.
4. Sartorelli, A.C. (1986). The role of mitomycin antibiotics in the chemotherapy of solid tumors. Biochem. Pharmacol. *35*, 67–69.
5. Iyer, V.N., and Szybalski, W. (1963). A Molecular mechanism of mitomycin action: linking of complementary DNA strands. Proc. Natl. Acad. Sci. USA *50*, 355–362.
6. Tomasz, M. (1995). Mitomycin C: small, fast and deadly (but very selective). Chem. Biol. *2*, 575–579.
7. Tomasz, M., Lipman, R., Chowdary, D., Pawlak, J., Verdine, G.L., and Nakanishi, K. (1987). Isolation and structure of a covalent cross-link adduct between mitomycin C and DNA. Science *235*, 1204–1208.
8. Pratt, W.B.R., Ensinminger, R.W., and Maybaum, W.D. (1994). The Anti-Cancerous Drugs, Second Edition (New York: Oxford University Press).
9. Uchida, I., Takasae, S., Kayakiri, H., Kiyoto, S., and Hashimoto, M. (1987). Structure of FR900482, a novel antitumor antibiotic from *Streptomyces*. J. Am. Chem. Soc. *109*, 4108–4109.
10. Inami, M., Kawamura, I., Tsujimoto, S., Nishigaki, F., Matsumoto, S., Naoe, Y., Sasakawa, Y., Matsuo, M., Manda, T., and Goto, T. (2002). Effects of FK317, a novel anti-cancer agent, on survival

of mice bearing B16BL6 melanoma and Lewis lung carcinoma. Cancer Lett. *181*, 39–45.

11. Naoe, Y., Inami, M., Matasumoto, S., Nishigaki, F., Tsujimoto, S., Kawamura, I., Miyayasu, K., Manda, T., and Shimomura, K. (1998). FK317: a novel substituted dihydrobenzoxazine with potent antitumor activity which does not induce vascular leak syndrome. Cancer Chemother. Pharmacol. *42*, 31–36.
12. Naoe, Y., Inami, M., Kawamura, I., Nishigaki, F., Tsujimoto, S., Matasumoto, S., Manda, T., and Shimomura, K. (1998). Cytotoxic mechanisms of FK317, a new class of bioreductive agent with potent antitumor activity. Jpn. J. Cancer Res. *89*, 666–672.
13. Naoe, Y., Inami, M., Takagaki, S., Matasumoto, S., Kawamura, I., Nishigaki, F., Tsujimoto, S., Manda, T., and Shimomura, K. (1998). Different effects of FK317 on multidrug-resistant tumor in vivo and in vitro. Jpn. J. Cancer Res. *89*, 1047–1054.
14. Naoe, Y., Inami, M., Matasumoto, S., Takagaki, S., Fujiwara, T., Yamazaki, S., Kawamura, I., Nishigaki, F., Tsujimoto, S., Manda, T., and Shimomura, K. (1998). FK317, a novel substituted dihydrobenzoxazine, exhibits potent antitumor activity against human tumor xenografts in nude mice. Jpn. J. Cancer Res. *89*, 1306–1317.
15. Naoe, Y., Kawamura, I., Inami, M., Matasumoto, S., Nishigaki, F., Tsujimoto, S., Manda, T., and Shimomura, K. (1998). Anti-cachectic effect of FK317, a novel anti-cancer agent, in colon26 and LX-1 models in mice. Jpn. J. Cancer Res. *89*, 1318–1325.
16. Beckerbauer, L., Tepe, J.J., Eastman, A.R., Mixter, F.P., Williams, R.M., and Reeves, R. (2002). Differential effects of FR900482 and FK317 on apoptosis, IL-2 gene expression, and induction of vascular leak syndrome. Chem. Biol. *9*, 427–441.
17. Tomasz, M., Lipman, R., Chowdary, D., Pawlak, J., Verdine, G.L., and Nakanishi, K. (1987). Isolation and structure of a covalently cross-link adduct between mitomycin C and DNA. Science *235*, 1204–1208.
18. Williams, R.M., Rajski, R.M., and Rollins, B.S. (1997). FR900482, a close cousin of mitomycin C that exploits mitosene-based DNA cross-linking. Chem. Biol. *4*, 127–137.
19. Millard, J.T., Weidner, M.F., Raucher, S., and Hopkins, P.B. (1990). Determination of the DNA cross-linking sequence specificity of reductively activated mitomycin C at single-nucleotide resolution-deoxyguanosine residues at CpG are cross-linked preferentially. J. Am. Chem. Soc. *112*, 3637–3641.
20. Sastry, M., Fiala, R., Lipman, R., Tomasz, M., and Patel, D.J. (1995). Solution structure of the monoalkylated mitomycin C-DNA complex. J. Mol. Biol. *247*, 338–359.
21. Li, V.-S., and Kohn, H. (1991). Studies on the bonding specificity for mitomycin C-DNA monoalkylation processes. J. Am. Chem. Soc. *113*, 275–283.
22. Kohn, H.L., Li, V.-S., Shiltz, P., and Tang, M.-S. (1992). On the origins of the DNA sequence selectivity of mitomycin monoalkylation transformations. J. Am. Chem. Soc. *114*, 9218–9220.
23. Judd, T.C., and Williams, R.M. (2002). Synthesis and DNA cross-linking of a phototriggered FR900482 mitosene progenitor. Org. Lett. *4*, 3711–3714.
24. Kumar, S., Lipman, R., and Tomasz, M. (1992). Recognition of specific DNA sequences by mitomycin C for alkylation. Biochemistry *31*, 1399–1407.
25. Richmond, T.J., and Davey, C.A. (2003). The structure of DNA in the nucleosome core. Nature *423*, 145–150.
26. Millard, J.T., Spencer, R.J., and Hopkins, P.B. (1998). Effect of nucleosome structure on DNA interstrand cross-linking reactions. Biochemistry *37*, 5211–5219.
27. Muthurajan, U.M., Park, Y.J., Edayathumangalam, R.S., Suto, R.K., Chakravarthy, S., Dyer, P.N., and Luger, K. (2003). Structure and dynamics of nucleosomal DNA. Biopolymers *68*, 547–556.
28. Krude, T. (1999). Chromatin assembly during DNA replication in somatic cells. Eur. J. Biochem. *263*, 1–5.
29. Tyler, J.K. (2002). Chromatin assembly. Cooperation between histone chaperones and ATP-dependent nucleosome remodeling machines. Eur. J. Biochem. *269*, 2268–2274.
30. Fyodorov, D.V., and Kadonaga, J.T. (2003). Chromatin assembly in vitro with purified recombinant ACF and NAP-1. Methods Enzymol. *371*, 499–515.
31. Anderson, M.G., and Dynan, W.S. (1994). Quantitative studies of the effect of HTLV-I Tax protein on CREB protein-DNA binding. Nucleic Acids Res. *22*, 3194–3201.
32. Kashanchi, F., Duvall, J.F., Kwok, R.P., Lundblad, J.R., Goodman, R.H., and Brady, J.N. (1998). The coactivator CBP stimulates human T-cell lymphotrophic virus type I Tax transactivation in vitro. J. Biol. Chem. *273*, 34646–34652.
33. Pan, S.S., Iracki, T., and Bachur, N.R. (1986). DNA alkylation by enzyme-activated mitomycin C. Mol. Pharmacol. *29*, 622–628.
34. Fletcher, T.M., Serwer, P., and Hansen, J.C. (1994). Quantitative analysis of macromolecular conformational changes using agarose gel electrophoresis: application to chromatin folding. Biochemistry *33*, 10859–10863.
35. Fletcher, T.M., Krishnan, U., Serwer, P., and Hansen, J.C. (1994). Quantitative agarose gel electrophoresis of chromatin: nucleosome-dependent changes in charge, sharp, and deformability at low ionic strength. Biochemistry *33*, 2226–2233.
36. Luger, K., Mader, A.W., Richmond, R.K., Sargent, D.F., and Richmond, T.J. (1997). Crystal structure of the nucleosome core particle at 2.8 Å resolution. Nature *389*, 251–260.
37. Rajski, S.R., Rollin, S.B., and Williams, R.M. (1998). FR66979 covalently cross-links the binding domain of the high-mobility group I/Y proteins to DNA. J. Am. Chem. Soc. *120*, 2192–2193.
38. Beckerbauer, L., Tepe, J.J., Cullison, J., Reeves, R., and Williams, R.M. (2000). FR900482 class of anti-tumor drugs cross-links oncoprotein HMG I/Y to DNA in vivo. Chem. Biol. *7*, 805–812.
39. Krude, T. (1995). Chromatin. Nucleosome assembly during DNA replication. Curr. Biol. *5*, 1232–1234.
40. Narlikar, G.J., Fan, H.Y., and Kingston, R.E. (2002). Cooperation between complexes that regulate chromatin structure and transcription. Cell *108*, 475–487.
41. Kaufman, P.D., Kobayashi, R., Kessler, N., and Stillman, B. (1995). The p150 and p60 subunits of chromatin assembly factor I: a molecular link between newly synthesized histones and DNA replication. Cell *81*, 1105–1114.
42. Nabatiyan, A., and Krude, T. (2004). Silencing of chromatin assembly factor 1 in human cells leads to cell death and loss of chromatin assembly during DNA synthesis. Mol. Cell. Biol. *24*, 2853–2862.
43. Dyer, P.N., Edayathumangalam, R.S., White, C.L., Bao, Y., Chakravarthy, S., Muthurajan, U.M., and Luger, K. (2004). Reconstitution of nucleosome core particles from recombinant histones and DNA. Methods Enzymol. *375*, 23–44.
44. Sambrook, J., and Russell, D.W. (2001). Molecular Cloning: A Laboratory Manual, Volume 2, Third Edition (New York: Cold Spring Habor Laboratory Press).
45. Cech, T.R. (1981). Alkaline gel electrophoresis of deoxyribonucleic acid photoreacted with trimethylpsoralen: rapid and sensitive detection of interstrand cross-links. Biochemistry *20*, 1431–1437.
46. Wongwisansri, S., and Laybourn, P.J. (2004). Reconstitution of yeast chromatin using yNap1p. Methods Enzymol. *375*, 103–117.